Optical Properties of Organic Hazes in Water-rich Exoplanet Atmospheres: Implications for Observations with JWST

Chao He, Michael J. Radke, Sarah E Moran, S. M. Hörst, Nikole Lewis, Julianne I. Moses, Mark S Marley, Eliza Miller Ricci Kempton, Caroline V Morley, Jeff A. Valenti, et al.

Optical Properties of Organic Hazes in Water-rich Exoplanet Atmospheres: Implications for Observations with *JWST*

Chao He[1*], Michael Radke[1], Sarah E. Moran[1,2], Sarah M. Hörst[1,3], Nikole K. Lewis[4], Julianne I. Moses[5], Mark S. Marley[2], Eliza M.-R. Kempton[6], Caroline V. Morley[7], Jeff A. Valenti[3], & Véronique Vuitton[8]

[1] Department of Earth and Planetary Sciences, Johns Hopkins University, Baltimore, MD, USA che13@jhu.edu

[2]Lunar and Planetary Laboratory, University of Arizona, Tucson, AZ, USA

[3]Space Telescope Science Institute, Baltimore, MD, USA

[4]Department of Astronomy and Carl Sagan Institute, Cornell University, Ithaca, NY, USA

[5]Space Science Institute, Boulder, CO, USA

[6]Department of Astronomy, University of Maryland, College Park, MD, USA

[7]Department of Astronomy, the University of Texas at Austin, Austin, TX, USA

[8]Institut de Planétologie et d'Astrophysique de Grenoble, Université Grenoble Alpes, CNRS, Grenoble, France

***JWST* has begun its scientific mission, which includes the atmospheric characterization of transiting exoplanets. Some of the first exoplanets to be observed by *JWST* have equilibrium temperatures below 1000 K, which is a regime where photochemical hazes are expected to form. The optical properties of these hazes, which controls how they interact with light, are critical for interpreting exoplanet observations, but relevant data are not available. Here we measure the optical properties of organic haze analogues generated in water-rich exoplanet atmosphere experiments. We report optical constants (0.4 to 28.6 μm) of organic hazes for current and future observational and modeling efforts covering the entire wavelength range of *JWST* instrumentation and a large part of *Hubble*. We use these optical constants to generate hazy model atmospheric spectra. The synthetic spectra show that differences in haze optical constants have a detectable effect on the spectra, impacting our interpretation of exoplanet observations. This study emphasizes the need to investigate the optical properties of hazes formed in different exoplanet atmospheres, and establishes a practical procedure to determine such properties.**

1. INTRODUCTION

Observations[1-6] indicate that many exoplanets could possess cloud and haze particles in their atmospheres and that these particles impact observed spectra. Recent modeling[7,8] and laboratory studies[9-12] suggest that organic haze particles are produced photochemically in temperate (<1000 K) exoplanet atmospheres, which are prime targets of observations for assessing habitability and searching for biosignatures beyond the Solar System. However, many exoplanets in this temperature range (including super-Earths and mini-Neptunes) have no Solar System analogs. The compositions and properties of organic hazes might be very distinct from what we know for Solar System bodies. These organic hazes can alter the transmission, emission, and reflected light spectra of exoplanets.[8,13] The optical properties of these hazes are essential to interpret exoplanet spectroscopic data and understand of their atmospheres.

Because the optical properties of exoplanet organic hazes are not yet known, the optical constants of Titan-like hazes (produced with 10% CH_4 in N_2) from Khare et al. (1984)[14] and of soots (carbonaceous particles formed from incomplete combustion of hydrocarbons)[15] are widely used to generate models and interpret observations.[8,16,17] In reality, the organic hazes formed in diverse atmospheres have a variety of compositions[18] and therefore diverse optical properties. The optical properties of Titan-like hazes or soots simply cannot represent the wide variety of atmospheric hazes we anticipate on exoplanets.[9-12] It is therefore necessary to measure the optical properties of organic hazes formed over a broad range of atmospheric conditions, given that JWST has begun to deliver unprecedented observations of various exoplanets.[6]

Exoplanets are expected to exhibit a wide diversity of atmospheric compositions. The signature of water is particularly sought on potentially habitable exoplanets because water is a key element for life on Earth. For example, water vapor has been detected in the atmosphere of a non-terrestrial exoplanet (K2-18 b) in the habitable zone.[19,20] Modeling studies[21-25] suggest that water worlds could be very common among low mass exoplanets

and there might be many water-rich atmospheres. Previous laboratory studies[9,10,18] have shown that water-rich atmospheres are likely to result in organic haze formation. Opacity from organic hazes can mask spectral features from water and other gases.[2,3,26,27] Here we measure the density and the optical properties of hazes analogous to those produced in temperate water-rich atmospheres. Their optical constants (the real refractive indices, n, and the extinction coefficients, k) are derived from 0.4 to 28.6 μm, covering optical wavelengths accessible with *Hubble* and ground-based facilities and the entire *JWST* wavelength range. Fig. 1 summarizes our experimental setup, the initial gas compositions and conditions, the measurements, and the analytical method of this study (for detailed information, see Methods).

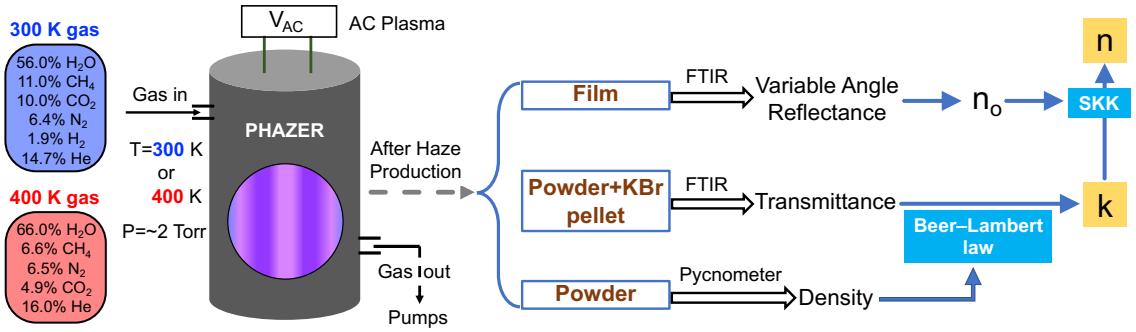

Fig. 1. Simplified schematic of the experimental setup, the simulated atmospheric compositions and conditions, the measurements, and the analytical method for the current study. Two haze analogues are produced with the PHAZER chamber by exposing the gas mixture (300 K or 400 K) to AC plasma energy source. These two gas mixtures represent the equilibrium compositions for atmospheres with 1000 times solar metallicity at 300 and 400 K, which are guided from chemical-equilibrium calculations (see Methods). The high haze production rate in these two gas mixtures[10] allows further analysis of the properties of the resulted haze particles. The density of the haze analogues is determined using a gas pycnometer, and their transmittance and reflectance spectra are measured with a Fourier transform infrared (FTIR) spectrometer. The extinction coefficients (k) are calculated based on the Beer-Lambert law, and the real refractive indices (n) are derived using the subtractive Kramers-Kronig (SKK) relation between n and k.

2. RESULTS

2.1. Density of Exoplanet Haze Analogues

The density of organic haze particles is an important property that impacts aerosol microphysics processes (coagulation, transport, and sedimentation) in exoplanet atmospheres. However, prior to this study the particle density was unknown due to lack of observational and experimental constraints. The haze mass density is often assumed to be 1 g cm^{-3} in many microphysics models[28-30], which is lower than the density we measured here. Our measurements here provide the first experimental constraints on the density of organic haze particles formed in water-rich exoplanet atmospheres, enabling realistic analysis and interpretation of observations of such exoplanets.

The measured densities are 1.328 and 1.262 g cm^{-3} (measurement uncertainties <1%) for the haze analogues from the simulated exoplanet atmospheres at 300 and 400 K, respectively. Their densities are lower than the haze analogues produced with the PHAZER chamber for icy bodies (1.35-1.43 g cm^{-3} for Titan, Triton, and Pluto haze analogues) in our Solar System.[31] The density differences reflect their distinct chemical compositions. Elemental analysis has shown that the two haze analogues for exoplanets have higher oxygen (>15% compared to <10%) but lower nitrogen (~22% compared to ~40%) contents relative to haze analogues for Titan, Triton and Pluto.[18,32] Besides the differences in elemental compositions, the chemical structures in each haze analogue, such as their molecular weight, polarity, and degree of unsaturation, also affect their density.

2.2. Transmittance of Exoplanet Haze Analogues and their Functional Groups

Exoplanet atmospheric transmission observations, obtained as the planet passes in front of host star, will be shaped by any hazes in the planet's atmosphere. Fig. 2 shows the transmittance of the two exoplanet haze analogues (300 and 400 K samples). For each sample, the transmittance spectra are obtained at three different concentrations in

potassium bromide (KBr) to capture both strong and weak absorption features. KBr is a typical carrier (as pellet or disk) for spectroscopy measurements because it is optically transparent from ultraviolet (0.22 μm) to far IR (~30 μm). As shown in Fig. 2, the general spectral shape and features are similar at both temperatures. They both have an absorption feature at 0.42 μm, suggesting that the samples contain aromatic compounds and/or unsaturated species with conjugated pi bonds.[33,34] The spectra are featureless from 0.5 to 2.5 μm but the absorption becomes weaker as the wavelength increases. Many absorption features appear from 2.5 to 20 μm due to bond vibrations of various organic functional groups in the haze analogues.

We expand this region in Fig. 2C to show the characteristic frequencies of different bonds. Fig. 2C identifies the bonds responsible for each spectral feature, including the characteristic absorptions of O–H, N–H, C–H, C≡N, –N=C=N–, C=O, C=N, C=C, N–O, C–O, and C–N bonds.[35,36] Table 1 summarizes the vibration modes of these bonds and their peak intensities. The absorption feature at 3500–2500 cm^{-1} (2.86–4.00 μm) is due to O–H bond stretching. This strong, broad feature indicates the predominance of alcohols (3500–3200 cm^{-1}) and carbonic acids (3300–2500 cm^{-1}) in the haze analogues. The stretching of N–H (3350–3300 and 3215–3190 cm^{-1}) and C–H (2965, 2933, 2875 cm^{-1}) bonds is present in this range as well but appears as relatively sharp peaks. Other absorption features in the spectra indicate the presence of nitriles, aromatics, and unsaturated and saturated organics in both the 300 and 400 K haze analogues. A small amount of carbodiimide compounds (–N=C=N–, ~2100 cm^{-1}) are only present in the 300 K haze sample, probably because lower temperature promotes carbodiimide formation from cyanamide.[37] Compared to Titan-like hazes[38,39], the exoplanet haze analogues in this study have obvious compositional differences, which include various oxygen-containing groups. This is not unexpected because there are two major oxygen-containing gases (H_2O and CO_2) in the initial atmospheres. The presence of oxygen-containing groups in the exoplanet haze analogues is supported by other analyses. Elemental analysis shows that these two haze analogues

have large oxygen contents (15% or 17% in mass), and high-resolution mass spectra reveal many oxygen-containing molecules in these samples.[18] The compositional difference leads to distinctive optical properties of the exoplanet haze analogues.

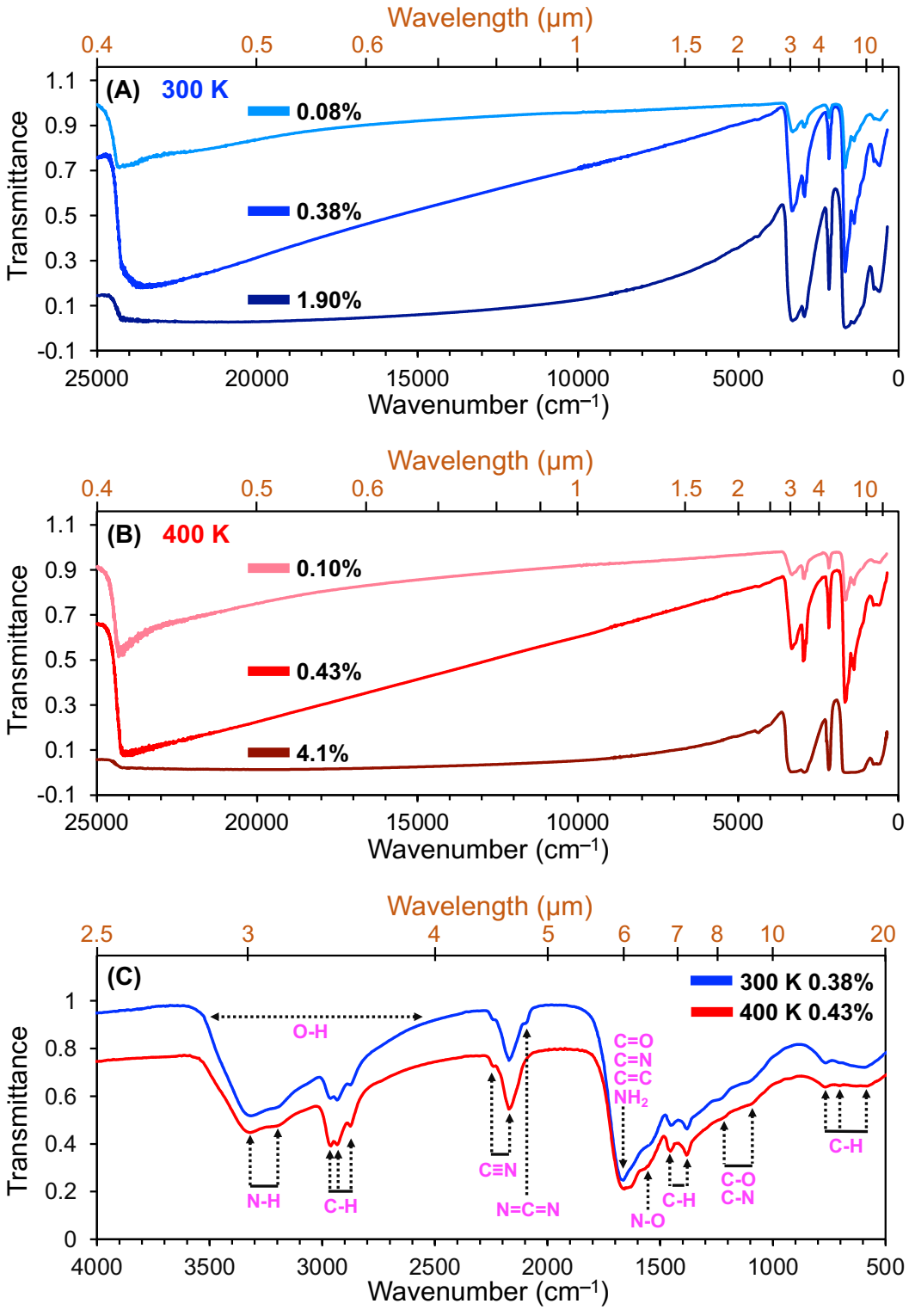

Fig. 2. The transmittance spectra of two exoplanet haze analogues formed in water-rich atmospheres at 300 K (A) and 400 K (B). The lines with different shades of color show the spectra of the samples with different concentrations in KBr (lighter color indicates lower concentration and darker indicates higher). The sample is mixed with KBr, and the percentage concentration is by mass. The transmittance spectra are obtained at different concentrations to capture both strong and weak absorption features in the samples. Panel C is the expansion of two spectra from panels A (0.38% of the 300 K sample) and B (0.43% of the 400 K sample) from 2.5 to 20 μm to show the absorption features of various functional groups. Different bonds are labeled in the figure near their absorption features.

Table 1. Functional group assignments to characteristic absorption frequencies of two exoplanet haze analogues as observed in the transmittance spectra (Fig. 2)

Frequency (ν) cm^{-1}	Wavelength (λ) μm	Functional group	Intensity
3500-2500	2.86-4.00	-O-H stretching, in alcohols and carbonic acids	strong, broad
3350-3300	2.98-3.03	-NH_2 or -NH- stretching	strong
3215-3190	3.11-3.13	-NH_2 stretching or overtone of NH_2 bending	strong
2965	3.37	-CH_3 asymmetric stretching	strong, sharp
2933	3.41	-CH_2- asymmetric stretching	strong, sharp
2875	3.48	-CH_3 symmetric stretching	strong, sharp
2244-2232	4.46-4.48	-C≡N or R-C≡C-R stretching	medium, shoulder
2172	4.60	Conjugated -C≡N stretching	strong, sharp
2108-2094	4.74-4.77	-N=C=N- stretching	medium, shoulder
1680-1626	5.95-6.15	C=O, C=N, C=C stretching or -NH_2 scissors bending	very strong
1580-1540	6.33-6.49	C=C stretching (aromatic) or N-O stretching (nitro)	medium, shoulder
1462-1450	6.84-6.90	sp^3 C-H bending	strong, sharp
1386-1378	7.21-7.26	sp^3 C-H bending or aldehydic C-H bending	strong, sharp
1247-1224	8.02-8.17	C-O or C-N stretching (aromatic)	weak, shoulder
1126-1104	8.88-9.06	C-O or C-N stretching (aliphatic)	weak, shoulder
775-762	12.9-13.12	sp^2 C-H bending	medium
714-701	14.0-14.26	sp^2 C-H bending	medium
612-584	16.34-17.12	sp^2 C-H bending	medium

2.3. Optical Constants of Exoplanet Haze Analogues

Optical constants for hazes can be used incorporate their features into theoretical spectra and for comparisons with retrieved values from observations. Fig. 3 shows the optical constants of two exoplanet haze analogues (300 and 400 K). The real refractive indices (n) are in the range between 1.43 and 1.82 for both samples, and the extinction coefficients (k) vary in a broad range from ~10^{-3} to 10^{-1}. The detailed data and their uncertainties can be found in Supplementary Information (Table S1). The uncertainties of the k values are estimated by considering the uncertainties of the transmittance measurements, the thickness calculations, and the average relative standard deviation of k values obtained for the samples at three different concentrations. For the n values, the uncertainties are determined from the error propagations of the uncertainty of n_0 at the anchor point and the integration of the k values. The uncertainties for the k values are about 1-4% at longer wavelengths (>2.9 μm) where the k values are larger than 0.01, but increase up to 9% at shorter wavelengths (0.4 to 2.9 μm) where the k values are smaller than 0.01. The determined n values have small uncertainties (3-4%) across the measured wavelength range because of the accuracy of the n_0 (uncertainty less than 1%) and the integration of the k values over the entire wavelength range. The n and k values of the two haze analogues (300 and 400 K) are similar in general and share many fine-scale features. Over most of the measured wavelength range, the 300 K sample has slightly lower n values but slightly higher k values relative to the 400 K sample. This could be caused by differences in their chemical compositions. For example, the 300 K sample has higher extinction coefficient at ~3 μm, indicating that it contains more N–H bonds. This is consistent with the elemental analysis that shows the 300 K sample has higher nitrogen content than the 400 K sample (27% vs 21%).[18] In addition, the higher extinction coefficients at 5.9-6.5 μm suggest that there are more double bonds in the 300 K sample.

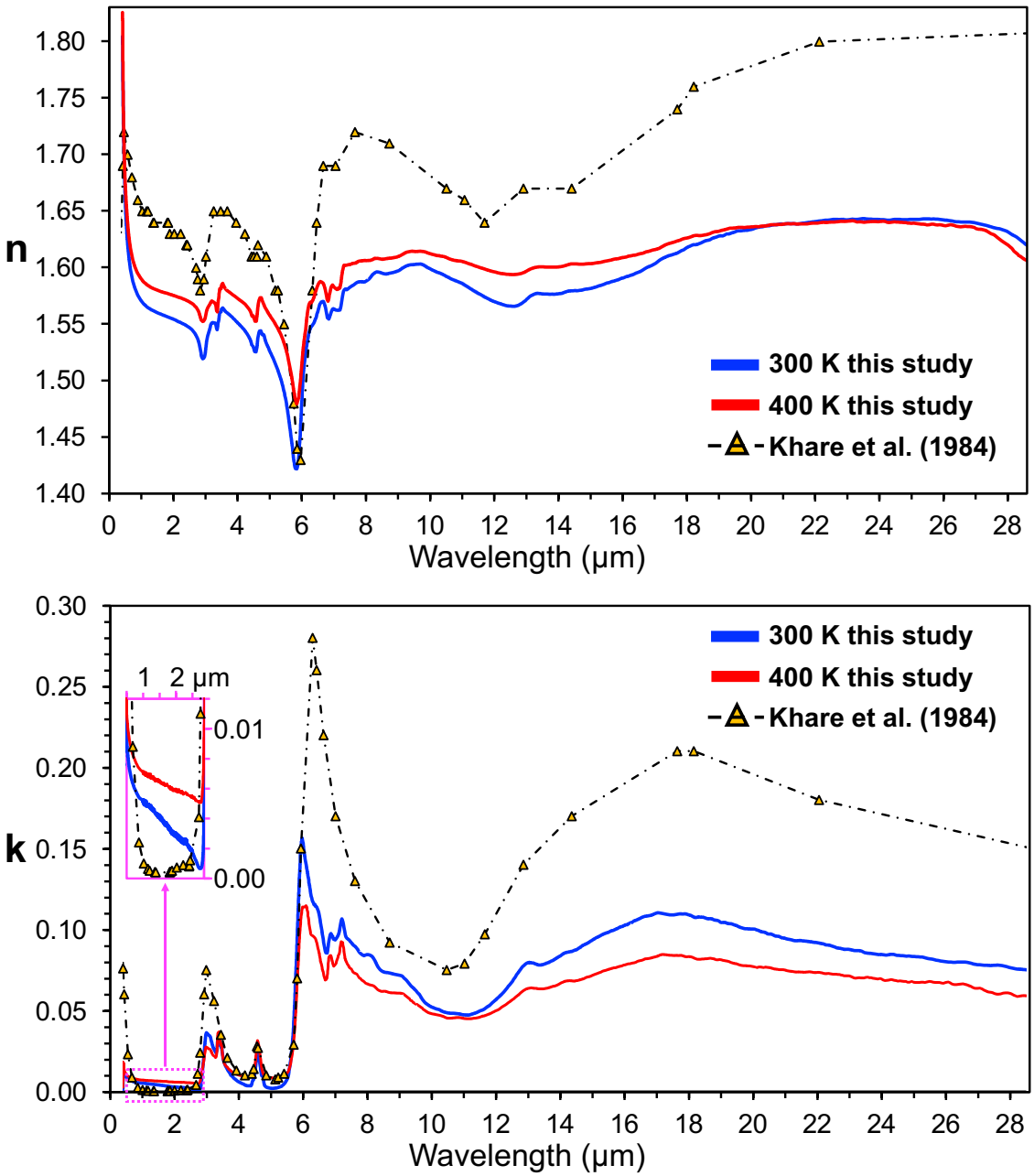

Fig. 3. Optical constants of two exoplanet haze analogues along with those of Titan-like hazes from Khare et al (1984): (A) the real refractive indices (n), and (B) the extinction coefficients (k) as function of wavelength (0.4 to 28.6 μm). The inset of (B) shows the difference of k values between this study and the one from Khare et al (1984), when k is smaller than 0.01 from 0.5 to 2.9 μm.

The optical constants of Titan-like hazes from Khare et al. (1984)[14] are also plotted in Fig. 3 for comparison. Due to its extensive spectral coverage (from soft X-ray, 0.025 μm, to

183 microwave frequencies, 1000 μm), the optical constants from Khare et al. (1984)[14] are
184 widely used in atmospheric modeling and observation interpretations for both Solar System
185 bodies (Titan[40], Triton[41], and Pluto[42]) and many exoplanets.[30,31,43] However, the haze
186 analogues used in Khare et al. (1984)[14] for the optical measurements were produced with
187 DC plasma discharge in N_2/CH_4 = 90/10 gas mixture at 0.2 mbar, with the purpose of
188 simulating haze particles formed in Titan's upper atmosphere.
189 As shown in Fig. 3, the general trend of the optical constants of two exoplanet haze
190 analogues in this study is similar to that of the Titan-like hazes from Khare et al. (1984)[14]
191 because of the organic nature of these materials. However, our *n* and *k* values are
192 substantially smaller than those of Khare et al. (1984)[14] over most of the measured
193 wavelength range. Both of our two samples have smaller n values than the Titan-like hazes
194 from Khare et al. (1984)[14] except at 5.8-6.2 μm where their n values are similar to those of
195 our 300 K sample. The k values from Khare et al. (1984)[14] at 0.4-0.6 μm, ~3 μm, and above
196 6 μm are about two times greater than our *k* values; they are comparable to the *k* values of
197 our 400 K sample from 3.4 to 5.8 μm; but they are smaller than our *k* values in the short
198 wavelength region (0.7-2.6 μm). Besides the differences of the absolute *n* and *k* values, the
199 data from Khare et al. (1984)[14] has fewer features than our values mainly due to two reasons.
200 First, the spectral measurements in Khare et al. (1984)[14] were done at very low resolution,
201 especially over the longer wavelengths (6-28.6 μm); second, the compositions are distinct
202 between our samples and those in Khare et al. (1984). The low-resolution can lead to fine
203 features not being resolvable (such as those from 6-10 μm), and the compositional
204 difference may cause some features to be weaker or absent (such as those at 3-3.5 μm).
205 The higher spectral resolution of the current study reveals new spectral features that may
206 enable measurements of haze composition, rather than just haze detection. Nonetheless, the
207 differences in the absolute values and the features can have consequential impacts on
208 atmospheric modeling and observational interpretation of exoplanets.

2.4. Effect of New Optical Properties of Exoplanetary Hazes on Atmospheric Transmission Spectra

We next briefly explore the effects of these newly derived exoplanet haze optical properties on transmission spectra for a representative exoplanet atmosphere. Since the experiments were run for hazy, water-rich atmospheres, we choose the parameters of the well-studied, likely aerosol-laden exoplanet GJ 1214 b as a reasonable example planet to demonstrate how our new optical properties would affect observations. GJ 1214 b has a mass of 8.17 ± 0.43 $M_{\oplus}$, a radius of 2.742 ± 0.05 $R_{\oplus}$, and an equilibrium temperature of 596 K.[44] The planet's mass and radius suggest its bulk density could be consistent with a hydrogen-rich atmosphere, or a steam atmosphere with a significant hydrogen/helium fraction[44] as in our experiments. The temperature is sufficiently warm that water should not condense out of the upper atmosphere. Observations with *Hubble* show its atmosphere has a featureless transmission spectrum from 1.1 to 1.7 microns, which could be indicative of a high altitude (~mbar) haze layer.[1] The incident UV flux is expected to drive significant photochemistry and potentially haze formation.[45,46]

Fig. 4 shows the synthetic spectra of a water-rich atmosphere reflecting the initial gas composition from the experiments at 400 K around a GJ 1214 b-like planet with the effects of a haze layer. We use the open-source aerosol modeling code *Virga*[47,48] and the open-source radiative transfer suite *PICASO*[49] to compute Mie properties for our hazes and implement them into a synthetic transmission spectrum model of an exoplanetary atmosphere (for detailed information about the haze modeling and generating the synthetic spectra, see Methods). We show spectra based on our newly derived optical properties for 300 and 400 K water-rich atmospheric hazes and for the commonly used Titan-like haze of Khare et al. (1984)[14]. Our aim in this work was to isolate the effect of the different haze optical properties on the atmospheric transmission spectra rather than perform a full model parameter study, and so we held all other haze parameters (e.g., particle size distribution, number density, vertical mixing) fixed. Interpretation of actual atmospheric spectral data

would require a full investigation into all these variables but is beyond the scope of this work.

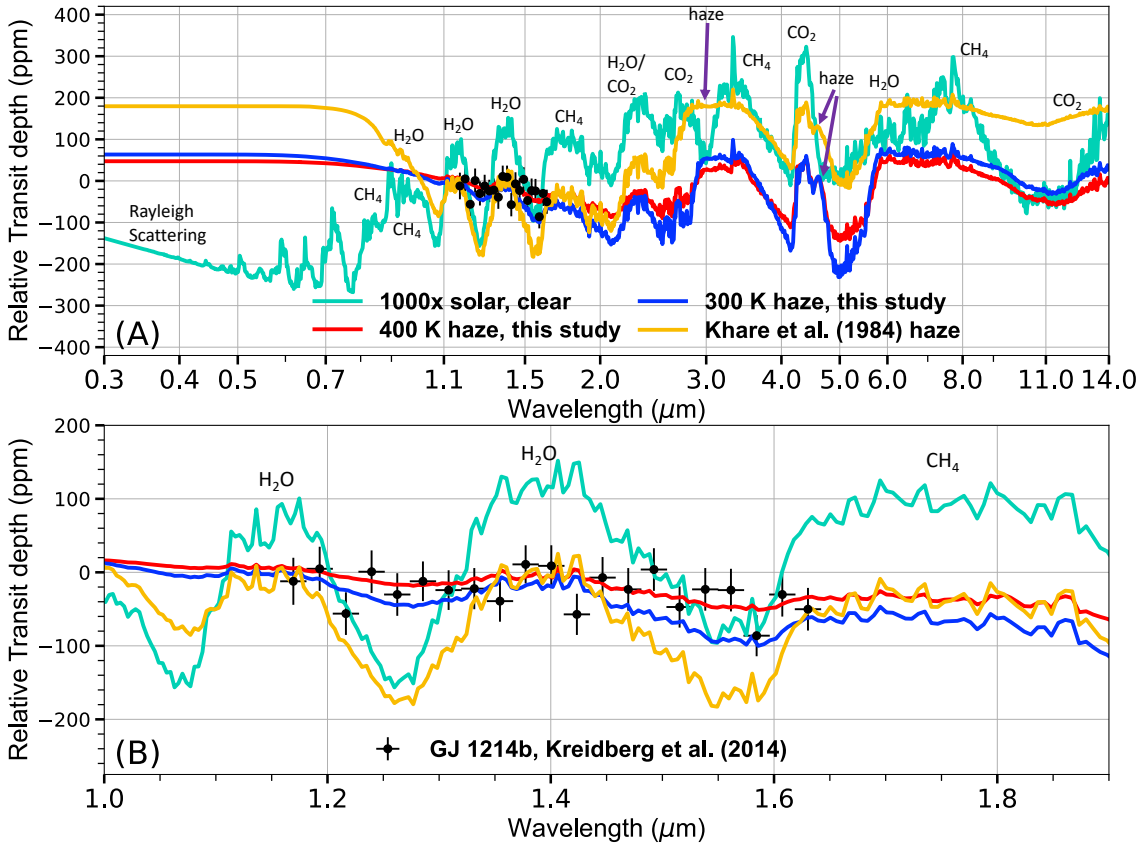

Fig. 4. Model spectra of a water-rich atmosphere around a GJ 1214 b -like planet, showing the effect of our newly measured haze optical properties. We also show the existing *Hubble* data of GJ 1214 b (Kreidberg et al. 2014)[1]. All spectra have been normalized by subtracting the mean of each transit depth from the spectrum, to better show the relative sizes of absorption features. The top panel (A) shows the spectra of our modeled atmospheres from 0.4 to 14 microns; bottom panel (B) shows our model atmospheres focused on *Hubble* Wide Field Camera 3/G141 instrument wavelengths. In teal, we show models of clear atmospheres with the laboratory atmospheric composition. Orange lines show hazy models generated using the optical properties for Titan-like hazes as measured by Khare et al. (1984). Red and blue lines show models generated using our newly derived optical properties for hazes made from 400 and 300 K water-rich atmospheres, respectively. The molecules and/or hazes responsible for the atmospheric features are indicated in each plot. **Given the same other atmospheric assumptions, the presence of our newly measured hazes would be differentiable from a Titan-like haze with observations from existing space-based observatories like *Hubble* and *JWST,* as with the GJ 1214 b data shown here.**

Throughout the spectrum, the values of n and k between our newly measured water-rich derived hazes and those of the Titan-like hazes[14] show similar behavior but at different intensities, as shown in Fig. 3. As such, all the hazy synthetic spectra we show in Fig. 4 mute the gaseous spectral features of the atmosphere, but to differing extents depending on the optical properties assumed for the haze particles. Notably, the Khare Titan-like hazes more heavily mute the atmospheric spectral features longward of 3.0 μm, while our water-rich hazes more heavily mute the atmospheric spectrum between 0.7 and 2.5 μm– that is, the wavelength region of focus for most *Hubble* exoplanet studies. In particular, the Titan-like hazes more strongly absorb at ~3 μm and ~6 μm, which probe functional groups due to amine (N-H) as well as carbon- and nitrogen-bearing (C=C, C=N, NH_2) bonds. The transit depth differences between haze models range from ~100 ppm in the mid-IR to ~150 ppm in the visible and near-IR, all of which are well within the sensitivity of *JWST* and *Hubble* measurements,[1,51-55] though this result relies on the same particle size distributions for the different kinds of hazes.

Additionally, the strength of the Rayleigh scattering slope from the visible towards the near-UV is enhanced by all hazes, though the Titan-like hazes absorb more strongly because of their larger k over the shortest wavelengths (0.4 to 0.7 μm). The difference between the visible-UV slopes of Titan-like and water-rich derived hazes is ~150 ppm for our modeled atmospheres. Smaller particles would enhance the variation between the visible-UV slopes (see Extended Data Fig. 3). Such differences are within the precision of Hubble's WFC3/UVIS instrument, which covers 0.2 to 0.8 μm. Since we have explicitly modeled the same haze particle size distributions and number densities for each set of optical properties, these differences here stem purely from the stronger absorption by the Titan-like haze over these wavelengths. In other words, using the optical properties from this study or from Khare et al. (1984)[14] to fit spectra from real observations would result in different inferred particle sizes and number densities for the same atmosphere to achieve the same scattering slope.

Most interestingly, our water-rich derived hazes almost completely mute the atmospheric spectrum over the HST WFC3/G141 bandpass, but the Titan-like haze of Khare et al. (1984)[14] allows the water and methane atmospheric features to peek through from 1 to 2 μm because its *k* values are an order of magnitude lower in the NIR. This results in our water-rich hazes providing a better match to the existing GJ 1214 b data from *Hubble*[1] compared to the Khare et al. (1984)[14] Titan-like hazes for the same abundance of haze mass loading. Both sets of haze optical properties allow atmospheric features to peek through at redder wavelengths which are covered by *JWST*. The size of these atmospheric features at longer wavelengths, even muted by haze, is still well within the precision of *JWST* measurement. Future model development and modeling studies, beyond the scope of this work, are needed to fully assess how vertical mixing and sedimentation of haze layers with these optical properties influence atmospheric spectra.

3. DISCUSSION

So far, the optical constants of the Titan-like hazes by Khare et al. (1984)[14] and various soots[15] have served as the only source for optical properties of organic haze in exoplanet atmospheres. Our study provides optical constants (0.4 to 28.6 μm) of organic hazes photochemically produced in water-rich exoplanet atmospheres. The optical constants of our water-rich derived exoplanet hazes differ from those of the Titan-like hazes[14], therefore affecting transmission, thermal emission, and reflected light spectra of exoplanets to different extents. When interpreting actual observations of exoplanets, using different optical constants of hazes can lead to different conclusions; in some cases, using inapplicable optical constants may lead to misinterpretations. Such misinterpretations could include incorrect atmospheric abundances of key species such as water and methane[56,57], or incorrect aerosol particle sizes and extents[30], which could then further affect the temperature structure[17] and thus the inferred dynamics and climate feedbacks within an atmosphere.[58]

JWST has an unprecedented capability to detect faint chemical signatures in exoplanet atmospheres and is set to observe a wide variety of exoplanet types. The haze particles formed in those exoplanet atmospheres are likely to have different compositions, which would then have distinct optical properties. The optical properties of different hazes are essential to interpreting observations, but we should be cautious when applying the existing haze optical constants to different types of exoplanets. In addition, the optical constant data of different hazes are necessary input parameters for atmospheric modeling of various exoplanets to understand their physical and chemical processes (i.e., their temperature structures, climates, etc.). The two sets of optical constants reported here are applicable for temperate water-rich exoplanet atmospheres and can be used for current and future observational and modeling efforts of such atmospheres. More laboratory work is needed to determine optical constants of haze analogues formed in various exoplanet atmospheric regimes. This study demonstrates a feasible avenue to determine such properties in the future.

4. METHODS

4.1 Production of Haze Analogues

The exoplanet haze analogues are produced using the Planetary Haze Research (PHAZER) experimental setup at Johns Hopkins University.[31] The detailed experimental procedure has been described previously.[9-12] This study uses haze analogues produced in the two water-rich atmospheres from our previous investigations.[9,10,18] The initial gas mixtures for our experiments are guided by the calculations from the chemical-equilibrium models of Moses et al. (2013).[59] Photochemical hazes are expected to play an important role in the atmospheres of exoplanets with equilibrium temperature below 1000 K, especially those planets with enhanced metallicities or enhanced C/O ratios.[7,9,10] The detailed compositions of actual exoplanet atmospheres have not yet been measured well, so we resort to chemical equilibrium calculations[59] to guide our experiments. The equilibrium atmospheric

compositions provide a reasonable starting point to investigate the photochemical processes in the atmospheres of super-Earths and mini-Neptunes with higher metallicity. In our previous studies[9-12], we explored atmospheres with a range of metallicities (100×, 1000×, and 10,000× solar metallicity) and equilibrium temperatures (300, 400, 600, and 800 K). The two water-rich atmospheres represent the equilibrium compositions for atmospheres with 1000× solar metallicity at 300 and 400 K. These two atmospheres produce haze at a higher rate than the other cases[10], which allows further analysis of the properties of the resulting haze particles.

Here, we briefly recount the production procedure. Gas mixtures, excluding water vapor, are premixed in a stainless-steel cylinder with high-purity gases purchased from Airgas (H_2-99.9999%, He-99.9995%, N_2-99.9997%, CH_4-99.999%, CO_2-99.999%). The total flow rate is 10 standard cubic centimeters per minute (sccm), and the premixed gas mixture flows at a proportional rate of 10 sccm based on the mixing ratio. Water vapor is introduced to the system at a pressure (corresponding to the mixing ratio) from HPLC water (Fisher Chemical) at the desired temperature maintained by a dry ice/methanol/water cold bath. A heating coil is employed to heat the gas mixture (including water vapor) to the experimental temperature (400 or 300 K). The gas mixture is then exposed to an AC glow discharge in a reaction chamber, which initiates complex chemical processes and leads to the formation of new gas-phase products and solid particles. After 72 hours of continuous discharge flow, we collect the haze analogues as powders and films on quartz substrate disks in a dry (<0.1 ppm H_2O), oxygen free (<0.1 ppm O_2), N_2 glove box (Inert Technology Inc., I-lab 2GB). The haze analogues are kept in the glovebox until further analysis to avoid contamination from Earth's atmosphere and light sources.

4.2 Density Measurements

The density of exoplanet haze analogues has not been reported previously. We determine the density of our haze analogues by measuring the mass and volume of a certain amount

of sample by using an analytical balance (±0.0001 gram) and a gas pycnometer (AccPyc II 1340, Micrometrics), respectively. We first fill the powder sample to ~70% of a 0.1 cm^3 cup and measure the mass of the sample in the cup on the balance (where the mass of the cup is known). Next, we measure the volume of the sample at ambient temperature with the gas pycnometer that uses the gas (helium) displacement method to determine the sample volume based on Boyle's law of volume–pressure relationships. We set the pycnometer to measure 20 cycles, and the average volume from the 20 measurements is reported with a standard deviation less than 0.0001 cm^3. The density is then calculated by dividing the mass by the volume.

4.3 Vacuum Fourier-transform Infrared Spectroscopy (FTIR) Measurement

We employ a Vertex 70v FTIR spectrometer (Bruker Optics) to characterize the spectral properties of the haze analogues. The Vertex 70v is a vacuum spectrometer, which can eliminate the spectral features (H_2O or CO_2 absorption) from Earth's atmosphere and increase the peak sensitivity without masking very weak spectral features. The wavelength range of the spectrometer is 0.4 to 28.6 μm (25,000 cm to 350 cm^{-1}) with a maximum resolution of 0.4 cm^{-1}, covering the whole observable wavelength range of *JWST* and a large part of *Hubble*. This spectrometer is configured with a Reflection/Transmission accessory (A510 Q/T, Bruker) and Seagull Variable Angle Reflection Accessory (Harrick Scientific), allowing transmittance measurements and reflectance measurements at different angles.

To derive the optical constants of the haze analogues, we measure the reflectance of the film samples on quartz discs and transmittance of the powder samples using the potassium bromide (KBr) pellet method. The films deposited on optical-grade quartz substrates in the reaction chamber are directly used for the reflectance measurements (4.3.1). The procedure for making KBr pellets is described in 4.3.2 and the transmittance measurements of the pellets are described in 4.3.3.

4.3.1 Reflectance Measurements of the films

Using the Seagull Variable Angle Reflection Accessory, we measure the reflectance of each haze analogue film at two different angles of incidence, 15° and 45°. The reflectance of the films on quartz substrates is measured under vacuum (below 0.2 mbar) at room temperature (294 K). We measure the reflectance in the wavelength range from 0.4 to 1.1 μm using a quartz beamsplitter and silicon diode detector. We acquire 1000 scans and average them to obtain spectra with a resolution of ~5 cm^{-1}. The reflectance of an aluminum standard mirror is measured as reference. The reflectance spectrum of the sample is the ratio of the sample measurement to the reference measurement.

4.3.2 Preparation of the KBr Pellets

A quality KBr pellet is critical for quantitative measurements. To ensure that the pellet is dry, KBr powder is dried in an oven overnight at 110 °C and immediately transferred to the dry N_2 glove box after heating. Subsequent pellet-making steps are all performed in the glove box. First, the KBr and the sample powders are separately ground to fine particles (< 2 μm) with ShakIR (a ball-mill grinder from Pike Technologies). Dry and fine KBr is used to make a pure KBr pellet as a spectral reference. The fine particles of the sample and KBr are mixed using the ShakIR to create a homogenous mixture of sample/KBr before making pellets.

The concentration of the sample in KBr needs to be optimized for transmittance measurements, usually between 0.5-3% depending on the absorption coefficients. Due to the complex nature of the haze analogues, we prepare the haze/KBr mixtures with three different concentrations to reveal both strong and weak absorption features in the samples. The actual concentrations of our mixtures range from 0.08 to 4.1%. Because the quantities of the haze analogues in the KBr pellet are relatively small, we use a two-step dilution method to minimize errors in the measurement process. As reported in Myers et al. (2019)[60], this method can reduce gravimetric error for the mass measurements from nearly 10% to

less than 1%. For example, to prepare a 0.1% mixture, we weigh 25 mg of the haze analogue using the analytical balance (±0.0001 gram) and mix it with 975 mg of KBr in the ShakIR to create a 2.5% mixture; next, we take 40 mg of the 2.5% mixture and 960 mg of pure KBr, and then mix them thoroughly using the ShakIR. After two dilutions, a 1:1000 (or 0.1%) homogenous sample/KBr mixture is ready to be pressed into a pellet.

Approximately 200 mg of finely ground KBr powder or homogenous mixture is placed into a 13 mm pellet die (Pike Technologies), and then is pressed on a CrushIR 15 Ton Digital Press (Pike Technologies). We apply 3 tons of force for 2 seconds, 7 tons for 30 seconds, and 10 tons for 120 seconds. The pressed pellet (diameter: 13 mm, thickness: ~0.5 mm) is removed from the die, mounted on a standard sample holder, and loaded into the FTIR spectrometer for transmittance measurement.

4.3.3 Transmittance Measurements of the Pellets

We measure the transmittance of the pressed pellets over a wavelength range from 0.4 to 28.6 μm under vacuum (below 0.2 mbar) at room temperature (294 K). Two detectors (silicon diode and DLaTGS detector) and two beamsplitters (quartz beamsplitter and KBr beamsplitter) are used to cover the whole wavelength range. The silicon diode detector and quartz beamsplitter are used from 0.4 to 1.11 μm (25000 to 9000 cm^{-1}); the DLaTGS detector and quartz beamsplitter are used from 0.83 to 1.25 μm (12000 to 8000 cm^{-1}); and the DLaTGS detector and KBr beamsplitter are used from 1.11 to 28.6 μm (9000 to 350 cm^{-1}). Overlapping data confirm that the spectrometer is calibrated properly across different wavelength ranges. For each measurement, 500 scans are acquired with a resolution of ~2 cm^{-1}. The transmittance of a pure KBr pellet is measured as a reference. The transmittance spectrum of the sample is the ratio of the sample measurement to the reference measurement.

4.4 Optical Constants Derivation

With the data from the measurements described above, we can derive the optical constants (complex refractive index, n+ik, where n is the real refractive index and k is the imaginary refractive index or the extinction coefficient) of the haze analogues. Based on the Beer-Lambert law, the absorbance (A) can be expressed as Equation 1 (Eq. 1):

$$A = \alpha(\nu) * d \quad \text{Eq. 1}$$

where α is absorption coefficient, ν is the wavenumber, and d is the effective thickness of the sample. The absorbance (A) can be determined from the FTIR measurements (Eq. 2):

$$A = -lnT = -ln\frac{I}{I_0} = ln\frac{I_0}{I} \quad \text{Eq. 2}$$

where T is the transmittance, I is the light intensity passing through the sample (haze/KBr pellet), and I_0 is the light intensity of the reference (pure KBr pellet). The effective thickness (d) of the sample in the pellet is equal to:

$$d = \frac{m}{\pi r^2 * \rho} \quad \text{Eq. 3}$$

in which m is the mass of the haze analogues in the pellet, r is the pellet radius (6.5 mm), and ρ is the measured density of the haze analogues.

Therefore, the absorption coefficient (α) can be calculated:

$$\alpha(\nu) = ln\frac{I_0}{I}/d \quad \text{Eq. 4}$$

Then, the extinction coefficient (k) can be determined:

$$k(\nu) = \frac{\alpha(\nu)}{4\pi\nu} = \frac{1}{4\pi\nu d} ln\frac{I_0}{I} \quad \text{Eq. 5}$$

For each sample, we obtain three sets of the extinction coefficients (k) independently by measuring the transmittance of three pellets with different effective thicknesses. The final k values are determined by averaging the three sets of k values.

With the determined extinction coefficient (k), we can calculate the real refractive index (n) based on the subtractive Kramers-Kronig (SKK) relation[61-63] between n and k as in Eq. 6:

$$n(\nu) = n_0 + \frac{2(\nu^2 - \nu_0^2)}{\pi} P \int_0^\infty \frac{\nu\prime k(\nu')}{(\nu\prime^2 - \nu^2)(\nu\prime^2 - \nu_0{}^2)} d\nu' \quad \text{Eq. 6}$$

where v is wavenumber (cm^{-1}), n_0 is the real refraction index at v_0, and P indicates the Cauchy principal value. The principal P value is integrated for the entire wavelength range; we use the k values calculated (Eq. 5) from 350 to 25000 cm^{-1} in the integrand and assume constant k values for wavelengths beyond the measured range. The assumption is generally valid unless there are large local absorption peaks outside the measurement range. Using an anchor point (n_0) can reduce the uncertainty for the numerical integration as demonstrated in previous studies.[62,63] However, the real refraction index of the haze analogues is initially unknown. From the interference fringes on the reflectance spectra of the film samples at two angles (15° and 45°) of incidence (see Extended Data Fig. 1), we determine n values from 0.4 to 1.1 μm using Eq. 7.

$$n_0 = \sqrt{\frac{sin^2\theta_1 * (\Delta v_1)^2 - sin^2\theta_2 * (\Delta v_2)^2}{(\Delta v_1)^2 - (\Delta v_2)^2}} \quad \text{Eq. 7}$$

where θ_1 and θ_2 are the two different angles of incidence in our reflectance measurements of the film samples (15° and 45°), and Δv_1 and Δv_2 are the average fringe spacing in the reflectance spectrum at respective incidence angle (θ_1 and θ_2). The n_0 value determined at 0.625 μm (v_0=16000 cm^{-1}) is used as the anchor point for the numerical integration in Eq. 6 to calculate the real refractive index (n) from 0.4 to 28.6 μm using the SKK relation. We used different anchor points (n_0 at different wavelengths) for the calculation and found that the yielded n values are very close (the difference is less than 2%).

4.5 Atmospheric Transmission Spectra Simulation

We use the open-source aerosol modeling code *Virga*[48] and the open-source radiative transfer suite *PICASO*[49] to compute haze Mie properties and implement them into a synthetic transmission spectrum model of an exoplanetary atmosphere. To generate hazy atmospheric model spectra, we require a stellar radius, planetary mass and radius, pressure-temperature profile, an atmospheric gas mixture, and haze profiles.

For the atmospheric composition of our synthetic spectra, we input the system parameters of GJ 1214 b for the stellar and planetary mass and radius[44] and the same gas mixing ratios as in the experimental run of the 400 K experiment shown in Fig. 1 into *PICASO*, using a

simple parametrized isothermal pressure-temperature profile at GJ 1214 b's T_{eq} of 600 K. Into *Virga*, we input the optical properties of our experimental hazes as their real and imaginary refractive indices *n* and *k*, binned down from the native measured resolution to a spacing of 10 nm, which we verify is still a fine enough sampling to capture the spectral features of the haze. We then used *Virga'*s optics functionality to generate wavelength-dependent Mie coefficients using haze particle size distributions as measured in the laboratory by He et al. 2018[64]. In addition to the optical properties and particle size of the experimental haze, we also need the vertical extent and mass loading of the haze layer within *Virga* in order to compute a synthetic atmospheric transmission spectrum with *PICASO*. *Virga* currently does not have the capability to self-consistently compute photochemical haze profiles. Therefore, for simplicity, we implement an isobaric haze layer from a pressure of 0.1 bar to 0.1 μbar with haze mass loading of ~25 particle/cm^3. These values are consistent with the extent of haze in Titan's mesosphere[65] as well as self-consistent haze formation modeling that has been performed for exoplanets.[66] The resulting optical depth of the wavelength-dependent haze layers as a function of pressure and wavelength from our model set-up is shown in Extended Data Fig. 2. For the Titan-like haze cases, we use the same settings as described above for our 400 K and 300 K haze layers, but substitute the refractive indices of Khare et al. (1984)[14].

The purpose of our spectra simulation is to show the effect of the different haze optical properties on the atmospheric transmission spectra rather than perform a full model parameter study. Simplified assumptions were used in our simulation, such as atmospheric pressure-temperature profiles, the particle radius and mass distribution. Future model development and modeling studies, employing self-consistent pressure-temperature profiles including the radiative effects of the haze[17], and full microphysics treatment of particle parameters[67-71], are required to fully explore haze impacts on observations of exoplanet atmospheres.

References

1. Kreidberg, L. et al. Clouds in the atmosphere of the super-Earth exoplanet GJ1214b. *Nature* **505**, 69–72 (2014).
2. Knutson, H. A., Benneke, B., Deming, D. & Homeier, D. A featureless transmission spectrum for the Neptune-mass exoplanet GJ436b. *Nature* **505**, 66–68 (2014).
3. Knutson, H. A. et al. Hubble space telescope near-IR transmission spectroscopy of the super-Earth HD 97658b. *Astrophys. J.* **794**, 155 (2014).
4. Lothringer, J. D. et al. An HST/STIs optical transmission spectrum of warm Neptune GJ 436b. *Astron. J.* **155**, 66 (2018).
5. Dragomir, D. et al. Rayleigh scattering in the atmosphere of the warm exo-Neptune GJ 3470b. *Astrophys. J.* **814**, 102 (2015).
6. JWST Transiting Exoplanet Community Early Release Science Team. Identification of carbon dioxide in an exoplanet atmosphere. *Nature* (2022). https://doi.org/10.1038/s41586-022-05269-w
7. Gao, P. et al. Aerosol composition of hot giant exoplanets dominated by silicates and hydrocarbon hazes. *Nat. Astron*. **4**, 951–956 (2020).
8. Morley, C. V., Fortney, J. J., Kempton, E. M. R., Marley, M. S., Visscher, C., & Zahnle, K. Quantitatively assessing the role of clouds in the transmission spectrum of GJ 1214b. *Astrophys. J.* **775**(1), 33 (2013).
9. He, C. et al. Photochemical haze formation in the atmospheres of super- Earths and mini-Neptunes. *Astron. J.* **156**, 38 (2018).
10. Hörst, S. M. et al. Haze production rates in super-Earth and mini-Neptune atmosphere experiments. *Nat. Astron.* **2**, 303–306 (2018).
11. He, C., Hörst, S. M., Lewis, N. K., et al. Sulfur-driven haze formation in warm CO2-rich exoplanet atmospheres. *Nat. Astron.* **4**, 986-993 (2020).
12. He, C., Hörst, S. M., Lewis, N. K., et al. Haze formation in warm H2-rich exoplanet atmospheres. *Planet. Sci. J.* **1**, 51 (2020).
13. Gao, P., Wakeford, H. R., Moran, S. E., & Parmentier, V. Aerosols in Exoplanet Atmospheres. *JGR: Planets* **126**(4), e06655, (2021).
14. Khare, B.N., et al. Optical constants of organic tholins produced in a simulated Titanian atmosphere: From soft X-ray to microwave frequencies. *Icarus* **60**, 127–137 (1984).
15. Chang, H. & Charalampopoulos, T. T. Determination of the Wavelength Dependence of Refractive Indices of Flame Soot. *In Proceedings of the Royal Society of London. Series A* **430**, 577–591 (1990).
16. Lavvas, P., & Koskinen, T. Aerosol properties of the atmospheres of extrasolar giant planets. *Astrophys. J.* **847**(1), 32 (2017).
17. Morley, C. V., Fortney, J. J., Marley, M. S., Zahnle, K., Line, M., Kempton, E., et al. Thermal emission and reflected light spectra of super Earths with flat transmission spectra. *Astrophys. J.* **815**(2), 110 (2015).

18. Moran, S. E. et al. Chemistry of temperate super-Earth and mini-Neptune atmospheric hazes from laboratory experiments. *Planet. Sci. J.* **1**, 17 (2020).
19. Tsiaras, A., Waldmann, I. P., Tinetti, G., Tennyson, J. & Yurchenko, S. N. Water vapour in the atmosphere of the habitable-zone eight-Earth-mass planet K2-18b. *Nat. Astron.* **3**, 1086–1091 (2019).
20. Benneke, B., Wong, I., Piaulet, C., Knutson, H. A., Lothringer, J., Morley, C. V., et al. Water vapor and clouds on the habitable-zone sub-Neptune exoplanet K2-18b. *Astrophys. J. Lett.* **887**(1), L14 (2019).
21. Mulders, G., Ciesla, F., Min, M. & Pascucci, I. The snow line in viscous disks around low-mass stars: implications for water delivery to terrestrial planets in the habitable zone. *Astrophys. J.* **807**, 9–15 (2015).
22. Kite, E. S. & Ford, E. B. Habitability of exoplanet waterworlds. *Astrophys. J.* **864**, 75–102 (2018).
23. Zeng, L. et al. Growth model interpretation of planet size distribution. *Proc. Natl Acad. Sci. USA* **116**, 9723–9728 (2019).
24. Kite, E. S. & Schaefer, L. Water on hot rocky exoplanets. *Astrophys. J. Lett.* **909**, L22 (2021).
25. Luque, R., & Pallé, E. Density, not radius, separates rocky and water-rich small planets orbiting M dwarf stars. *Science* **377**, 1211-1214 (2022).
26. Chachan, Y., Jontof-Hutter, D., Knutson, H. A., Adams, D., Gao, P., Benneke, B., et al. A featureless infrared transmission spectrum for the super-puff planet Kepler-79d. *Astrophys. J.* **160**(5), 201 (2020).
27. Libby-Roberts, J. E., Berta-Thompson, Z. K., Désert, J.-M., Masuda, K., Morley, C. V., Lopez, E. D., et al. The featureless transmission spectra of two super-puff planets. *Astron. J.* **159**(2), 57 (2020).
28. Adams, D., Gao, P., de Pater, I. & Morley, C. V. Aggregate hazes in exoplanet atmospheres. *Astrophys. J.* **874**, 61 (2019).
29. Gao, P., & Zhang, X. Deflating Super-puffs: Impact of photochemical hazes on the observed mass-radius relationship of low-mass planets. *Astrophys. J.* **890**(2), 93 (2020).
30. Ohno, K., & Tanaka, Y. A. Grain growth in escaping atmospheres: Implications for the radius inflation of super-puffs. *Astrophys. J.* **920**(2), 124 (2021).
31. He, C. et al. Carbon monoxide affecting planetary atmospheric chemistry. *Astrophys. J. Lett.* **841**, L31 (2017).
32. Moran, S. E. et al. Triton haze analogs: The role of carbon monoxide in haze formation. *JGR-Planets* **127**, e2021JE006984 (2022).
33. Rao, C. N. R. Ultra-violet and visible spectroscopy: chemical applications, Butterworths, London, pp. 242 (1975).
34. van Krevelen D. W. & te Nijenhuis K. Chapter 10: Optical Properties, in Properties of Polymers, Elsevier, Oxford, UK, pp. 287-320 (2009).

35. Lin-Vien, D., Colthup, N. B., Fateley, W. G. & Grasselli, J. G. The Hand- book of Infrared and Raman Characteristic Frequencies of Organic Molecules. Academic Press, San Diego. 503 p (1991).
36. Socrates, G. Infrared and Raman Characteristic Group Frequencies. Wiley, Chichester. 347 p (2001).
37. Duvernay, F., et al. Carbodiimide production from cyanamide by UV irradiation and thermal reaction on amorphous water ice. *J Phys Chem A.* **109**(4), 603-608 (2005).
38. Khare, B. N., et al. Analysis of the time-dependent chemical evolution of Titan haze tholin. *Icarus* **160**(1), 172-182 (2002).
39. Imanaka, H., et al. Laboratory experiments of Titan tholin formed in cold plasma at various pressures: implications for nitrogen-containing polycyclic aromatic compounds in Titan haze. *Icarus* **168**(2), 344-366 (2004).
40. Vinatier, S., et al. Optical constants of Titan's stratospheric aerosols in the 70–1500 cm− 1 spectral range constrained by Cassini/CIRS observations. *Icarus* **219**(1), 5-12 (2012).
41. Ohno, K., Zhang, X., Tazaki, R., & Okuzumi, S. Haze formation on Triton. *Astrophys. J.* **912**(1), 37 (2021).
42. Zhang, X., Strobel, D. F., & Imanaka, H. Haze heats Pluto's atmosphere yet explains its cold temperature. *Nature* **551**(7680), 352-355 (2017).
43. Arney, G. N., et al. Pale orange dots: the impact of organic haze on the habitability and detectability of Earthlike exoplanets. *Astrophys. J.* **836**(1), 49 (2017).
44. Cloutier, R., et al. A More Precise Mass for GJ 1214 b and the Frequency of Multiplanet Systems Around Mid-M Dwarfs. *Astron. J.* **162**, 174 (2021).
45. Lora, J.M., et al. Atmospheric Circulation, Chemistry, and Infrared Spectra of Titan-like Exoplanets around Different Stellar Types. *Astrophys. J.* **853**, 58 (2018).
46. Teal, D.J., et al. Effects of UV Stellar Spectral Uncertainty on the Chemistry of Terrestrial Atmospheres. *Astrophys. J.* **927**, 90. (2022).
47. Ackerman, A.S. & Marley, M.S. Precipitating Condensation Clouds in Substellar Atmospheres. *Astrophys. J.* **556**, 872-884 (2001).
48. Rooney, C.M., et al. A New Sedimentation Model for Greater Cloud Diversity in Giant Exoplanets and Brown Dwarfs. *Astrophys. J.* **925**, 33 (2022).
49. Batalha, N.E., et al. Exoplanet Reflected-light Spectroscopy with PICASO. *Astrophys. J.* **878**, 70 (2019).
50. Ohno, K. & Kawashima, Y. Super-Rayleigh Slopes in Transmission Spectra of Exoplanets Generated by Photochemical Haze. *Astrophys. J. Lett.* **895**, L47 (2020).
51. Ahrer, E.-M., et al., Atmospheric water and chemistry in the exoplanet WASP-39b with JWST NIRCam. *Nature*, in press (2022).
52. Alderson, L., et al., The molecular inventory of the exoplanet WASP-39b with JWST NIRSpec G395H. *Nature*, in press (2022).
53. Feinstein, A.D., et al. Atmospheric composition and clouds in the exoplanet WASP-39b with JWST NIRISS. *Nature*, in press (2022).

54. Rustamkulov, Z., et al., A panchromatic spectrum of the exoplanet WASP-39b with JWST NIRSpec PRISM. *Nature*, in press (2022).
55. Sing, D.K., et al., A continuum from clear to cloud hot-Jupiter exoplanets without primordial water depletion. *Nature* **529**, 7584 (2016).
56. Lupu, R. E., Marley, M. S., Lewis, N., Line, M., Traub, W. A., & Zahnle, K. Developing atmospheric retrieval methods for direct imaging spectroscopy of gas giants in reflected light. I. Methane abundances and basic cloud properties. *Astron. J.* **152**(6), 217 (2016).
57. Lacy, B., Shlivko, D., & Burrows, A. Characterization of exoplanet atmospheres with the optical coronagraph on WFIRST. *Astron. J.* **157**(3), 132 (2019).
58. Steinrueck, M. E., et al. 3D simulations of photochemical hazes in the atmosphere of hot Jupiter HD 189733b, *Monthly Notices of the Royal Astronomical Society* **504**(2), 2783–2799 (2021).
59. Moses, J. I. et al. Compositional diversity in the atmospheres of hot Neptunes, with application to GJ 436b. *Astrophys. J.* **777**, 34 (2013).
60. Myers, T. L., et al. Obtaining the complex optical constants n and k via quantitative absorption measurements in KBr pellets. *Chemical, Biological, Radiological, Nuclear, and Explosives (CBRNE) Sensing XX*. 11010. SPIE (2019).
61. Wood, B. E., & Roux, J. A. Infrared optical properties of thin H_2O, NH_3, and CO_2 cryofilms. *JOSA,* **72**(6), 720-728 (1982).
62. Toon, O. B., et al. Infrared optical constants of H_2O ice, amorphous nitric acid solutions, and nitric acid hydrates. *JGR-Atmospheres* **99**(D12), 25631-25654 (1994).
63. Imanaka, H., Cruikshank, D. P., Khare, B. N., & McKay, C. P. Optical constants of Titan tholins at mid-infrared wavelengths (2.5–25 μm) and the possible chemical nature of Titan's haze particles. *Icarus* **218**(1), 247-261 (2012).
64. He, C. Hörst, S.M., Lewis, N.K., et al. Laboratory Simulations of Haze Formation in the Atmospheres of Super-Earths and Mini-Neptunes: Particle Color and Size Distribution. *Astrophys. J. Lett.* **856,** 1 (L3). 2018.
65. Lavvas, P., Yelle, R.V., and Vuitton, V. The detached haze layer in Titan's mesosphere. *Icarus* **201** (2), 626-633 (2009).
66. Kawashima, Y. & Ikoma, M. Theoretical Transmission Spectra of Exoplanet Atmospheres with Hydrocarbon Haze: Effect of Creation, Growth, and Settling of Haze Particles. I. Model Description and First Results. *Astrophys. J.* **853**, 7 (2018).
67. Trainer, M.G., et al. The Influence of Benzene as a Trace Reactant in Titan Aerosol Analogs. *Astrophys. J. Lett.* **766,** L4 (2013).
68. Lavvas, P., et al. Aerosol growth in Titan's Ionosphere. *Proc. Natl Acad. Sci. USA* **110**, 8 (2013).
69. Yoon, Y.H., et al., The Role of Benzene Photolysis in Titan Haze Formation. *Icarus* **233**, 233-241 (2014).
70. Gao, P. & Benneke, B. Microphysics of KCl and ZnS Clouds on GJ 1214 b. *Astrophys. J.* **863**, 165 (2018).

71. Ohno, K. & Okuzumi, S. A Condensation-Coalescence Cloud Model for Exoplanetary Atmospheres: Formulation and Test Applications to Terrestrial and Jovian Clouds. *Astrophys. J.* **835**, 261 (2017).

Acknowledgements

This work was supported by the NASA Astrophysics Research and Analysis Program NNX17AI87G and the NASA Exoplanets Research Program 80NSSC20K0271. We thank Natasha Batalha for very helpful conversations and troubleshooting with the *Virga* model.

Author contributions

C.H., M.R., S.E.M., S.M.H., N.K.L., M.S.M., and J.I.M. conceived the study. J.I.M. calculated the starting gas mixtures. C.H. carried out the experiments. C.H. and M.R. performed the optical measurements. S.E.M. and C.H. simulated the synthetic transmission spectra. C.H. conducted the data analysis and prepared the manuscript. All authors participated in discussions regarding interpretation of the results and edited the manuscript.

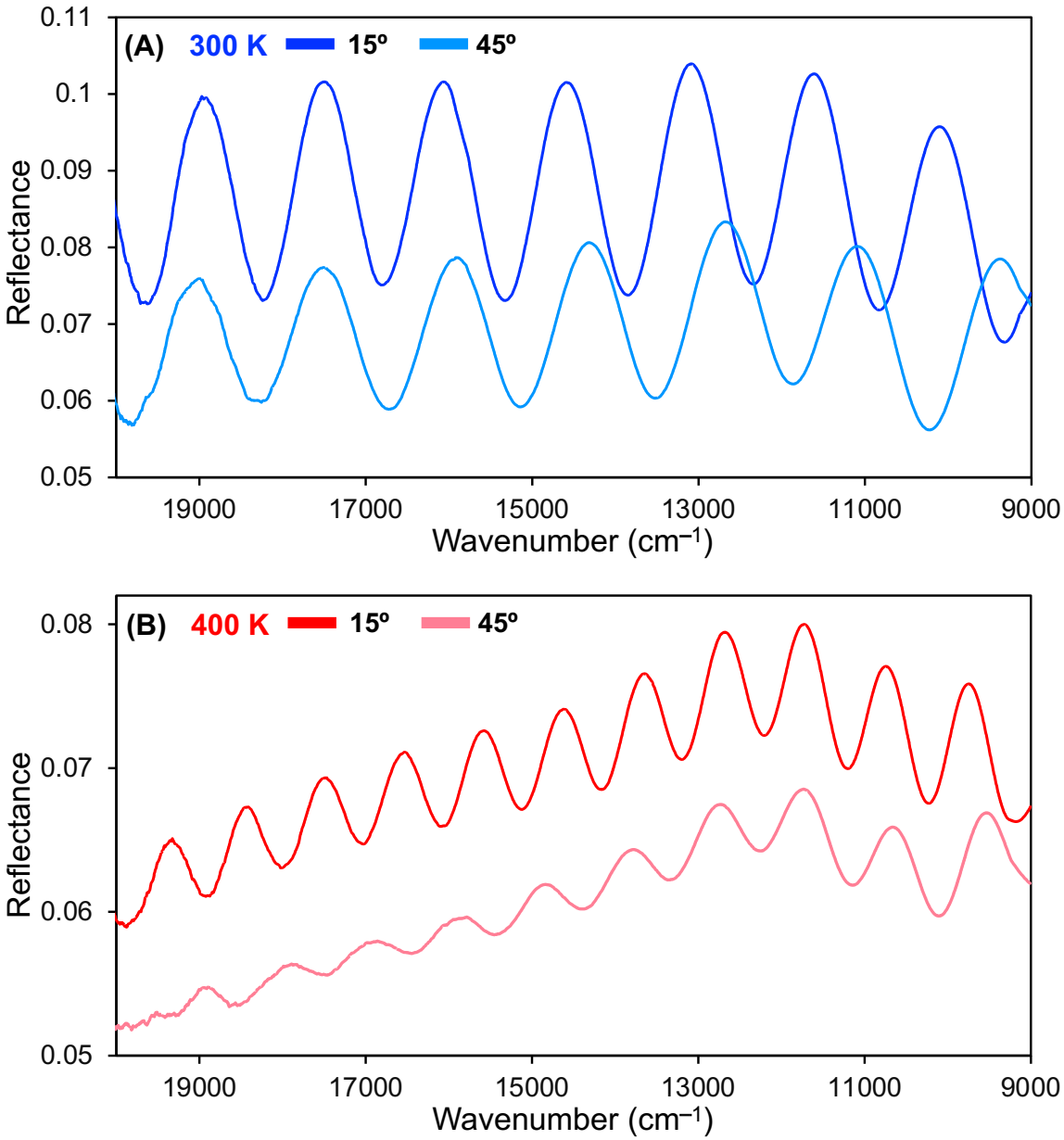

Extended Data Fig. 1. Reflectance spectra of two exoplanet haze analogues formed in water-rich atmospheres at 300 K (A) and 400 K (B). Using Seagull Variable Angle Reflection Accessory, we measure the reflectance of each haze analogue film at two different angles of incidence, 15° (darker shade) and 45° (lighter shade). The spectra from 20000 to 9000 cm^{-1} (0.5 to 1.1 μm) are shown here. From the interference fringes on the reflectance spectra at two different angles, the *n* values of the samples at corresponding wavelengths can be determined using Eq. 7.

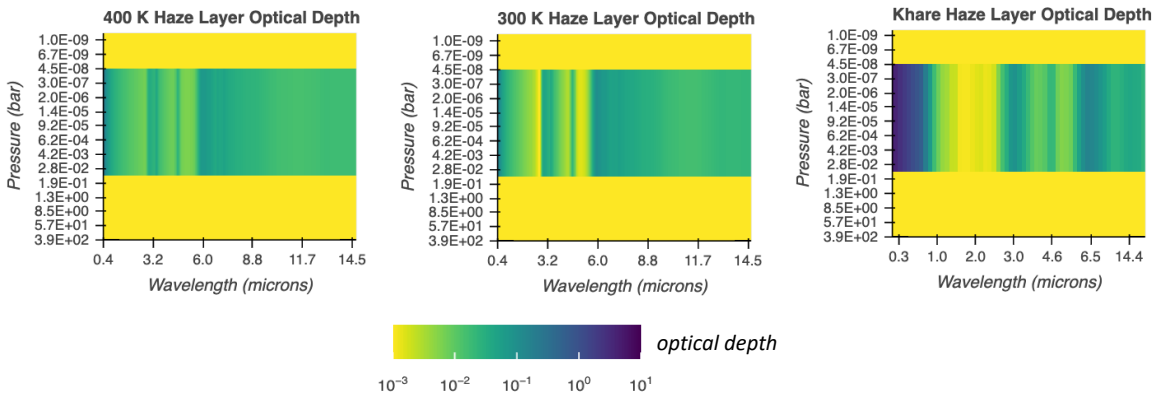

699

700 **Extended Data Fig. 2**. Haze slab profiles as a function of pressure and wavelength as
701 implemented with the *Virga*-derived Mie coefficients. The color bar indicates the optical
702 depth at each wavelength, with darker shading corresponding to higher optical depths. The
703 haze layer extends from 0.1 bar to 0.1 μmbar with a haze particle radii distribution centered
704 around 25 nm. Note that the Khare et al. (1984) data has wider wavelength coverage than
705 shown, but at lower resolution than our measured optical properties.
706

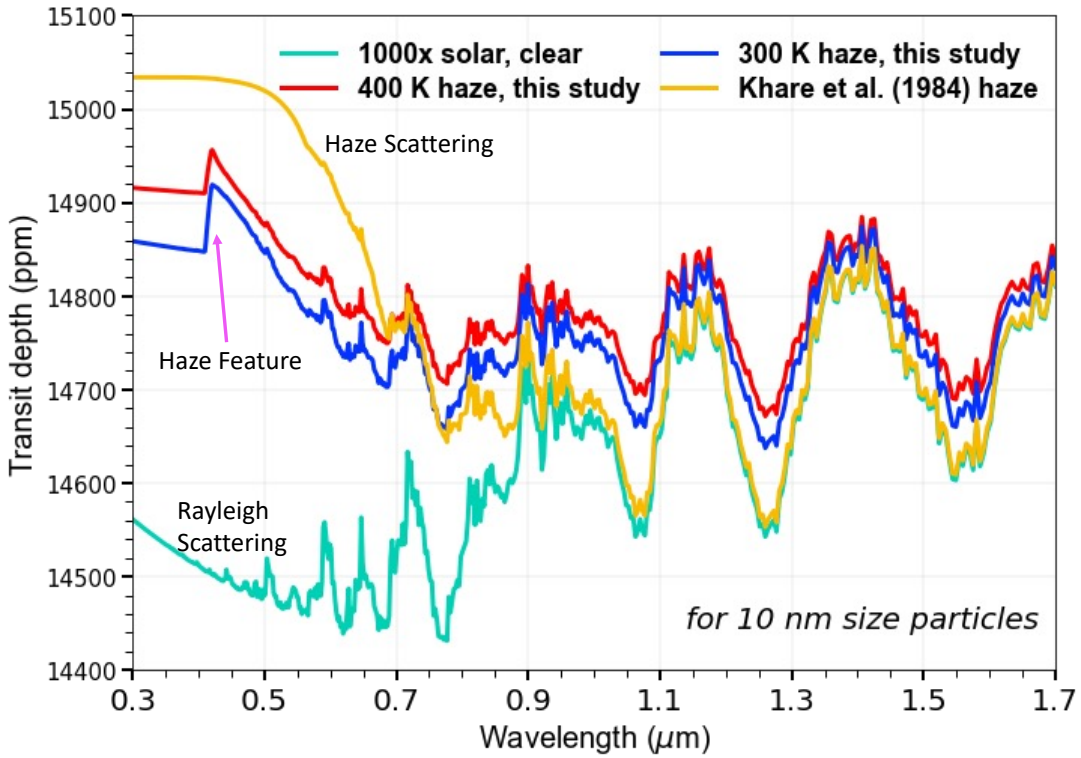

707

708 **Extended Data Fig. 3.** Model spectra of a water-rich atmosphere around a GJ 1214 b -like
709 planet. We show the effect of our newly measured haze optical properties using small radii
710 (10 nm) haze particles, focusing on the wavelength range accessible to *Hubble*. The method

and settings for generating the spectra here are the same as described in 4.5, except the haze particle radii (10 nm) and haze mass loading (4 particles/cm^3). With sufficiently small particles, the large scattering slopes between different haze compositions are differentiable with *Hubble*'s ultraviolet/visible capabilities even if such hazes less strongly impact the NIR.